JAAS
www.rsc.org/jaas

Compensation for matrix effects in ICP-AES by using air segmented liquid microsample introduction. The role of the spray chamber

José Luis Todolí,[a] S. E. Maestre[a] and J. M. Mermet[a,b]

[a]*Departamento de Química Analítica, Nutrición y Bromatología, Universidad de Alicante, 03080 Alicante, Spain*
[b]*Laboratoire des Sciences et Stratégies Analytiques (CNRS-FRE 2394), Université Claude Bernard-Lyon, F-69622 Villeurbanne Cedex, France*

Received 5th January 2004, Accepted 16th March 2004
First published as an Advance Article on the web 17th May 2004

The combination of sample injection into an air carrier stream (*i.e.*, air segmentation) with a low sample consumption system has been evaluated for the analysis of microsamples through ICP-AES. A PFA micronebulizer has been coupled to: *(i)*, a double pass spray chamber; *(ii)*, a Cinnabar cyclonic spray chamber; and *(iii)*, a torch integrated sample introduction system, TISIS. Three matrices have been studied: in addition to water two concentrated acid solutions (2 mol l^{-1} nitric acid and 1.7 mol l^{-1} acetic acid) and Na 5,000 μg ml^{-1}. A simulation of the evolution of the drop size distributions of the aerosols with time was carried out in order to evaluate the extent of solvent evaporation inside the chamber. The total mass of solvent evaporated inside the chamber was estimated and it was concluded that, at 25 °C, about 4–6 s residence time were required to promote the maximum evaporation of the solvent. In order to ensure this, discrete sample introduction into an air carrier stream (*i.e.*, air segmentation) was used. Narrow peaks (*i.e.*, with a full width at half maximum, FWHM, as short as 10 s) were obtained for a 10 μl injected sample. The peaks found for the Cinnabar and TISIS were narrower than those for the double pass spray chamber. More importantly, the interferences caused by inorganic as well as organic matrices were less severe in discrete than in continuous mode. The theoretical simulations allowed explanation of these results in terms of the enhancement of the solvent evaporation both for water and matrices in this operating mode. The enhanced solvent evaporation with respect to the situation in continuous mode minimized differences in analyte transport towards the plasma induced by these compounds. Despite this, in discrete mode a residual matrix effect was found that was attributed to the aerosol transport process. Internal standardization (IS) was applied to transient signals and the interferences were compensated for in virtually all the cases. Good results were obtained for the four emission lines taken as internal standards (*i.e.*, Mg 280.270, Co 228.616, Cr 205.552 and Cu 324.754). However, for acetic acid and a few lines, IS was not efficient for removing interferences. The methodology was validated by analyzing two reference solid samples of foods (*i.e.*, bovine liver and mussel tissue). By using Cd 214.438 as internal standard and under discrete mode 100% recoveries were found.

In the field of ICP techniques, the analysis of microsamples is an issue of recent interest.[1] Among the different methods, the use of a micronebulizer coupled to a low inner volume spray chamber has reached acceptance because of its simplicity and reliability.[2] Pneumatic micronebulizers are widely used for applications requiring consumption of only several microliters of solution per minute. As regards the spray chamber, besides double pass designs, the so called Cinnabar has been extensively used for the analysis of microsamples.[3,4] The Cinnabar chamber is of cyclonic type but has a low inner volume so as to shorten the wash out times and to minimize the severity of memory effects. Recently, single pass spray chambers have proved to give rise to better analytical figures of merit and less severe matrix effects than both double pass and Cinnabar devices.[5] Owing to their simplicity, single pass spray chambers can be successfully used for the discrete introduction of liquid samples into the plasma.[6]

Sub-milliliter samples can also be analyzed by means of discrete techniques such as the injection of a sample plug into a carrier liquid or gas stream. The introduction of very low liquid sample volumes using air as a carrier presents several advantages over injection of the sample into a liquid stream.[7,8] Among them we can mention the drastic reduction in sample dispersion. Besides, it has been claimed that this technique also provides increased sample throughput and enhanced precision.[9] The reported sensitivity when injecting liquid samples into air is higher than when the analysis is performed by using a liquid carrier. The reasons used to explain this trend can be summarized as follows:[7,10] *(i)*, the dispersion of the sample plug is reduced; *(ii)*, analyte transport efficiency increases; *(iii)*, the energy transfer from the plasma to the aerosol is modified; and *(iv)*, the net plasma solvent load decreases. Although the background with air as carrier is higher than that for a water carrier stream, the enhancement in sensitivity leads to a reduction of the limits of detection in the former case. As regards the applications of sample injection in a gas stream or air segmentation, it maybe highlighted its use for carrying out on line slow reactions while ensuring a negligible sample dispersion[11] or the analysis of heterogeneous samples (whole blood).[8] Nonetheless, provided that there is no carrier solution, severe memory effects can be produced with this technique.[7] In order to reduce them, several injections of a clean solution must be performed. Another choice consists of the use of a water–air segmented stream.[12] The so-called air segmented discrete introduction technique has been used to mitigate the memory effects.[7,13] In this case, the sample is either injected into an air–segmented water carrier stream or sandwiched between two air bubbles and two small volumes of water. Despite its numerous advantages, no report has appeared dealing with the effect of the sample injection method on the

DOI: 10.1039/b317082a

interferences caused by organic as well as inorganic compounds in ICP-AES.

The combination of air stream sample injection with the use of very low sample consumption introduction systems could be a powerful methodology for the analysis of sub-milliliter samples by ICP techniques. The goals of the present work are: *(i)*, to evaluate the suitability of three different liquid sample introduction systems for the analysis of low sample volumes, *ca.* 10 μl, following the solution injection into an air stream; *(ii)*, to study the extent of the ICP-AES matrix effects in discrete mode and to compare it with the results obtained in continuous mode; and *(iii)*, to apply the air stream sample injection in combination with the internal standard technique for the analysis of reference food samples.

Experimental

A micronebulizer made of PFA polymer (PFA-ST, CPI International, The Netherlands) was used throughout. This nebulizer was coupled to a conventional Ryton-made double pass (100 cm^3, PerkinElmer, Uberlingen, Germany) spray chamber and a Cinnabar (20 cm^3, Glass Expansion, Australia). A torch integrated sample introduction system, TISIS, was used as well. The design, characteristics and relevant issues of this device have been described elsewhere, both in ICP-AES[14,15] and ICP-MS.[16] In the present work the TISIS was equipped with either 8 or 20 cm^3 inner volume cavities. The liquid delivery rate (Q_l) was controlled by using 0.25 mm id Tygon capillaries and a Gilson Minipuls 3 peristaltic pump (Villiers Le Bel, France).

Primary aerosols (*i.e.*, those generated by the nebulizer) and tertiary aerosols (*i.e.*, those leaving the spray chamber) were characterized by means of a sizer based on the Fraunhofer diffraction of a laser beam (Malvern Instruments, Malvern Worcestershire, UK). This system was equipped with a 63 mm lens focal length that enabled the apparatus to measure droplets within the 1.2–118 μm diameter range. For measurement of primary aerosols, the PFA nebulizer was placed at 6 mm from the beam center, whereas for tertiary aerosols measurement, the exit of the spray chamber was located at 5 mm from the beam. The complete volume drop size distributions were obtained as a function of time at a frequency of one reading per second.

Emission signal measurements were performed with a PerkinElmer Optima 3000 ICP-AES instrument (Überlingen, Germany) based on the radial viewing mode. Table 1 summarizes the plasma instrumental conditions. Table 2 lists the wavelengths as well as the excitation energies of the atomic lines and the ionic lines' energy sum values, E_{sum} (*i.e.*, the sum of the ionization and excitation energies) of the tested elements. The discontinuous introduction of the sample was performed by pumping the solution for a period of time. For measurement of the ICP-AES signal, the sample was aspirated at a rate of 60 μl min^{-1} for 10 s which gave a 10 μl injected volume. Prior to each injection the inner chamber walls were allowed to dry completely.

A 10 μg ml^{-1} multielemental solution (Merck IV) was used to determine the signal for different lines. Multielemental solutions were prepared in distilled water and in the presence of sodium 5000 μg ml^{-1}, nitric acid 2 mol l^{-1} and acetic acid 1.7 mol l^{-1}. Two BCR certified food solid reference materials were used to test the applicability of the discrete mode for the analysis of real samples: *(i)*, a bovine liver, ref. CRM 185R; and, *(ii)*, a mussel tissue, ref. CRM 278R.

Table 1 ICP-AES instrumental conditions

Rf power/kW	1.45
Integration time/ms	20
Sampling time/ms	1000
Outer gas flow rate/l min^{-1}	15
Intermediate gas flow rate/l min^{-1}	0.75
Central gas flow rate/l min^{-1}	0.7
Viewing height above load coil/mm	5

Table 2 Elements, wavelengths and E_{sum} (for ionic lines) or E_{exc} (for atomic lines)

Element	Wavelength/nm	E^{ab}/eV
Cr II	205.552	12.80
Zn I	213.856	5.80
Cd II	214.438	14.77
Co II	228.616	13.70
Ni I	232.003	5.34
Ba II	233.527	11.22
Fe II	238.204	13.07
Fe II	239.562	13.09
Mn II	257.610	12.25
Mg II	280.270	12.07
Mg I	285.213	4.35
Cu I	324.754	3.82

[a] For ionic lines: E_{sum} (sum of ionization and excitation energy). [b] For atomic lines: E_{exc} (excitation energy).

The digestion was conducted into a microwave oven (CEM 1000 MSP, Matthews, NC, USA). For a given sample, three 0.5 g portions were placed inside closed PTFE reactors. Then, the digestion solution (*i.e.*, 5 ml of distilled water + 5 ml of 65% nitric acid) was added. The digestion program was the same as that described previously.[17] Once the digestion was accomplished, the three samples were filtered and mixed, and the total volume of the resulting solution was adjusted to 50 ml with concentrated nitric acid. This was done in order to ensure that the matrix (*i.e.*, nitric acid and inorganic salts) would cause significant interferences. Because the concentration of many elements was very low, 10 g of each sample solution were spiked, after the digestion step, by adding 20 μl of the 1000 μg ml^{-1} multielement solution to match with the sensitivity of ICP-AES. The composition of the spiked reference materials is summarized in Table 3. Finally, the samples were analyzed with the ICP-AES instrument by using plain water standards.

Results and discussion

When a sample plug is nebulized into a dry environment, it is dispersed into the spray chamber. The droplet concentration along the plug is modified, being lower at the two plug extremes

Table 3 Elemental composition of the spiked reference samples

Sample	Element	Concentration in solid/μg g^{-1}
Bovine liver (CRM 185R)	Cd[a]	67.2
	Cu[a]	344
	Mn[a]	77.7
	Pb[a]	66.8
	Zn[a]	205
	Co[b]	66.7
	Ni[b]	66.7
	Li[b]	66.7
	Ba[b]	66.7
	Cr[b]	66.7
Mussel Tissue (CRM 278R)	Cu[a]	76.1
	Mn[a]	74.4
	Pb[a]	68.7
	Zn[a]	83.1
	Co[b]	66.7
	Ni[b]	66.7
	Li[b]	66.7
	Ba[b]	66.7
	Cr[a]	67.4

[a] Certified elements. [b] Added elements.

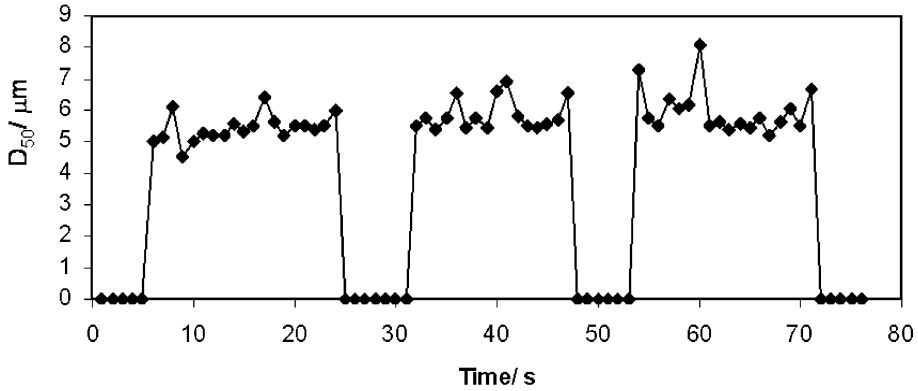

Fig. 1 Median of the primary aerosol volume drop size distribution *versus* time for distilled water. $Q_l = 200$ µl min^{-1}; $Q_g = 0.7$ l min^{-1}; sample injected volume = 60 µl.

than in the center. As a consequence, the liquid to gas volume ratio varies with time. Furthermore, provided that there is no solvent on the walls of the spray chamber, the solvent is evaporated only from the aerosol droplets. Therefore, by following the sample injection in an air stream procedure, the solvent evaporation is going to be promoted with respect to both continuous mode and when the sample volume is injected into a liquid carrier stream. Obviously, the longer the aerosol residence time inside the chamber, the more significant the solvent evaporation.

Aerosol characteristics

An interesting point when working with discrete sampling methods is to determine the time required for the stabilization of the aerosol production. Fig. 1 shows the variation of the median of the primary aerosol volume drop size distribution (D_{50}) *versus* time for three consecutive 60 µl injections of distilled water. It can be observed that the D_{50} values reach a steady value in a period of time inferior to one second.

Tertiary aerosol properties were also monitored for the matrices tested when working in discrete sample introduction. Fig. 2 shows the variation of the tertiary aerosols, D_{50} *versus* time, for the double pass spray chamber (Fig. 2a) and the TISIS operated with the 8 cm^3 cavity (Fig. 2b). In all cases, 60 µl of sample were injected in the air stream. By comparing these two figures, it can be observed that for the TISIS, the plots were noisier than for the double pass spray chamber. This was accounted for by the fact the TISIS used a low inner volume single pass chamber. Therefore, the aerosol trajectory towards the plasma was easier than with the double pass spray chamber. This allowed coarse droplets to escape and caused a shift of the volume median distribution towards higher values. Furthermore, the fluctuations produced during the aerosol generation step were not as efficiently dampened as in the case of the double pass spray chamber. Despite this, the average D_{50}

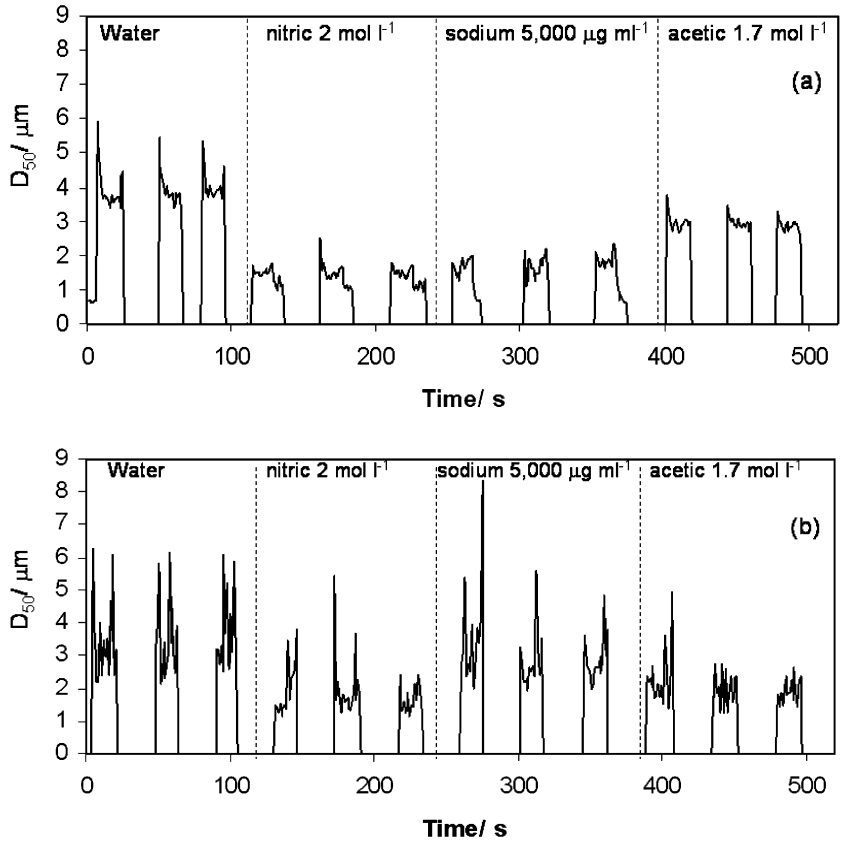

Fig. 2 Median of the tertiary aerosol volume drop size distribution *versus* time for the matrices tested when using the double pass spray chamber (a) and the TISIS equipped with the 8 cm^3 inner volume cavity (b). $Q_l = 200$ µl min^{-1}; $Q_g = 0.7$ l min^{-1}; sample injected volume = 60 µl.

values were similar for both systems and very close to the primary ones (Fig. 1). The PFA micronebulizer could be thus considered as an efficient device.[18]

As has already been indicated, inorganic and organic acids caused a change in the tertiary aerosol characteristics that were due to differences in the primary aerosols as well as modifications in the physical properties of the solution.[19] Fig. 2a shows that tertiary aerosols were finer for the three matrices studied than for distilled water. Nitric acid and sodium solutions changed the tertiary D_{50} more significantly than the acetic acid one. This behavior was somewhat different in the case of the TISIS (Fig. 2b), because it can be seen that, for this system, the tertiary aerosol D_{50} values were less influenced by the matrix nature than for the double pass spray chamber. In order to illustrate this, the D_{50} was registered *versus* time by continuously aspirating the solutions. For the double pass spray chamber, the tertiary D_{50} were 3.6, 1.4 and 1.5 μm for water, nitric and sodium, respectively. In the case of the TISIS with the 8 cm^3 cavity, the respective values were 2.8, 2.5 and 1.5 μm.

As regards the peak duration, from Fig. 2 it can be observed that the peaks found for both sample introduction systems were similar. The peaks lasted 18–20 s (*i.e.*, the same duration than primary ones). However, in the case of nitric acid and the double pass spray chamber, the signals were about 6 s wider. Several studies have demonstrated that nitric acid solutions are responsible for severe memory effects (*i.e.*, equilibration effects).[20] This trend was observed only for the double pass spray chamber. For the Cinnabar and TISIS, the peaks for tertiary aerosols had the same duration as those for primary aerosols. This observation agreed with previous reports in which the transient effects for these two systems were less significant than for the double pass spray chamber.[17]

At low liquid flow rates and in discrete mode, the relative extent of the processes occurring inside the spray chamber was different with respect to that under continuous mode and at conventional liquid flow rates. The solvent evaporation was expected to be enhanced and the coalescence of droplets dampened in the former situation. In the present work, a theoretical study was performed in order to evaluate the extent of the solvent evaporation and the evolution of the aerosol characteristics as the sample plug was nebulized into a dry chamber at liquid flow rates of several tens of microliters per minute.

The variation of the diameter of a droplet with time as a result of the solvent evaporation can be described according to the following equation:[21,22]

$$d^3 = d_0^3 - E\,t \tag{1}$$

where d is the drop diameter at a given time t, d_0 is the initial drop diameter and E is the so-called evaporation factor, which is given by:

$$E = \frac{48 D_v \sigma p_s M^2}{(\rho R T)^2} \tag{2}$$

where D_v is the diffusion coefficient for solvent vapour, σ is the solvent surface tension, p_s the saturated vapour pressure, M the molecular mass of the solvent, ρ the solvent density, R is the gas constant and T is the absolute temperature. Eqns. (1) and (2) have several simplifying assumptions, the most important of which are that the aerosol inside the chamber is under isothermal conditions and its flow regime is laminar.[22]

The measurement sizer used in the present work is equipped with a 31 rings detector, able to classify the aerosol diameters in 31 different categories or size ranges. In the present work, the volume drop size distribution of the aerosol generated by the nebulizer was obtained in frequency. Then, eqn. 1 was applied to each drop size range. As a result, the evolution of the x-axis with time was obtained. For a given drop size range (i), the aerosol liquid volume of the droplets was calculated as a function of time according to:

$$V_i = \frac{4}{3}\pi R_i^3$$
$$V_i = \frac{1}{6}\pi\left[(d_0)_i^3 - Et\right] \tag{3}$$

where R_i and $(d_0)_i$ are the mean radius and diameter for each drop size range, respectively. For each initial diameter, $(d_0)_i$, the volume was calculated at different times (eqn. 3). Then, each one of these volumes was divided by the initial volume, thus giving information about the fraction of solvent not evaporated (NE) for each size range.

$$\mathrm{NE} = \frac{V_i}{(V_0)_i} \tag{4}$$

Finally, this relative parameter was multiplied by the percentage of liquid volume in the band from the drop size distribution and by the liquid flow rate (the results were obtained by assuming a 30 μl min^{-1} delivery flow rate). The final result indicated the aerosol liquid volume flow rate (AL) contained in each size range at a given time.

$$\mathrm{AL} = 30\,\mathrm{NE}(\%\,\text{in band})$$
$$\mathrm{AL} = 30\left[1 - \frac{Et}{(d_0)_i^3}\right](\%\,\text{in band}) \tag{5}$$

Fig. 3 shows the absolute volume drop size distribution curves at three different times for water (Fig. 3a) and 2 mol l^{-1} nitric acid solution (Fig. 3b). The maximum time studied was 10 s, which corresponded to the estimated aerosol residence

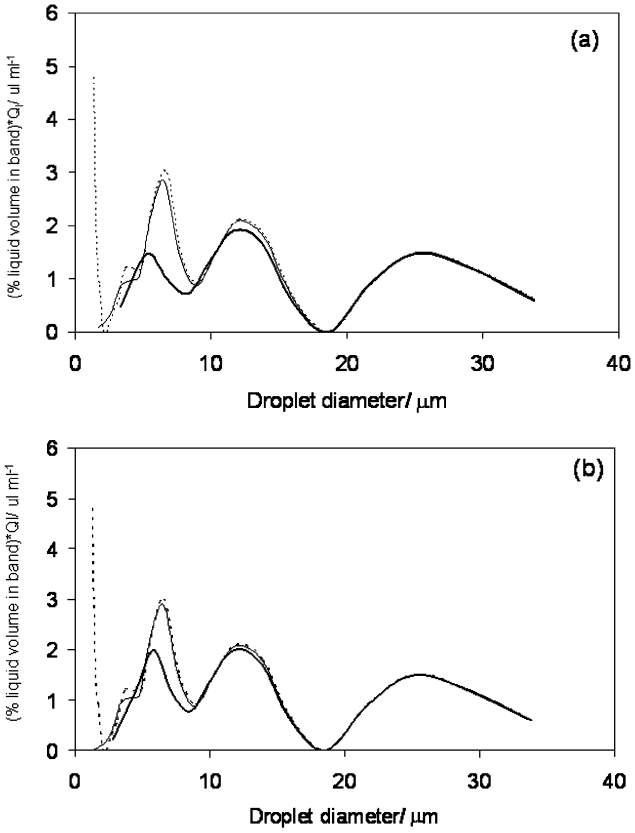

Fig. 3 Simulation of the evolution of the drop size distribution with time caused by solvent evaporation. (a) Distilled water; (b) 2 mol l^{-1} nitric acid. Q_l = 30 μl min^{-1}; Q_g = 0.7 l min^{-1}. Dotted line: primary aerosol distribution; continuous line: simulated aerosol distribution after 1 s; bold line: aerosol distribution after 10 s. All calculations performed at 25 °C.

time in a double pass spray chamber at the gas flow rate used (*i.e.*, 0.7 l min^{-1}). It can be observed that, according to our calculation, after 1 s all droplets with diameters lower than about 2 μm were completely evaporated (Fig. 3a), whereas the changes were almost negligible for droplets with diameters higher than about 9 μm. This expected trend confirmed that the small droplets evaporated faster than the bigger ones.

If the solution contained a matrix such as nitric acid, the solvent evaporation was dampened mainly as a result of the decrease in vapor pressure and the increase in the density. In fact, the corresponding evaporation factors (eqn. 2) were 1.5×10^{-2} and 1×10^{-2} μm^3 ms^{-1} for distilled water and 2 mol l^{-1} nitric acid, respectively. The drop size distribution changes for nitric acid solutions (Fig. 3b) were less significant than for distilled water. For the former matrix, after 10 s the changes in the distribution curves for droplets included within the 5–10 μm range were less pronounced than for water (Fig. 3a). The results obtained when considering the 5000 μg ml^{-1} Na solution were identical to those for the aqueous solution, because both evaporation factors were virtually equal.

The consequence of the solvent evaporation is the disappearance of fine droplets (*i.e.*, generation of coarse aerosols) until the coarsest droplets start to significantly decrease their diameters (*i.e.*, the aerosols become finer). In the present work, the median of the volume drop size distribution (D_{50}) was calculated from the data generated through the procedure mentioned before. At 10 s residence time the D_{50} calculated from the theoretically generated drop size distributions took values of about 6 and 11 μm for water and 2 mol l^{-1} nitric acid, respectively. This forecast did not correlate with the experimental data. Thus, the measured D_{50} values for the aerosols leaving a double pass spray chamber were 3.5 and 1.5 μm for distilled water and 2 mol l^{-1} nitric, respectively. These findings suggested that the evaporation was not the only phenomenon leading to a differentiation of tertiary aerosols as a function of the matrix and that other factors, such as coarse droplets removal through impacts against the chamber walls and droplet fission by electrical repulsion, could play a key role in terms of matrix effects.[23] Besides, it is important to bear in mind that the simulation performed in the present study has some inherent approximations.[17,22]

From the data presented in Fig. 3, it could be possible to estimate the total solvent volume evaporated as a function of time. To this end, the absolute volume drop size distribution curves were integrated for several aerosol residence times. Fig. 4 shows the results obtained for water and the 2 mol l^{-1} nitric acid solution. The grey area of this figure represents the volume of water that would evaporate at 25 °C temperature at the gas flow rate tested (*i.e.*, 0.7 l min^{-1}).[24] It can be seen that the maximum amount of water that could evaporate was reached at a residence time close to 6 s. According to these theoretical calculations, longer residence times would not promote further solvent evaporation. It is interesting to note that, provided that the spray chamber walls were allowed to dry before the sample injection, under discrete mode, the solvent volume evaporated mainly from the aerosol. Meanwhile, as it has been suggested,[20] in continuous mode, a significant fraction of the solvent evaporated from the solution on the chamber inner walls. It is also worth mentioning that, according to Fig. 4, after about 4–6 s residence time the amount of water evaporated was the same for the two matrices considered.

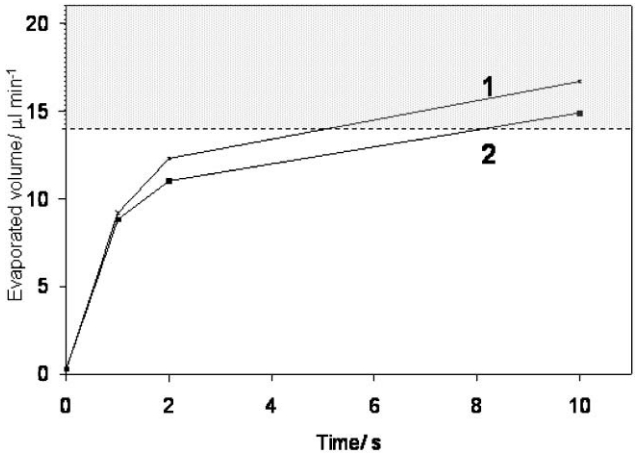

Fig. 4 Estimated evaporated water volume from the aerosol for distilled water (1) and 2 mol l^{-1} nitric acid (2). The data were obtained by integration of the drop size distribution curves generated from eqn 5. All calculations were performed at 25 °C.

Analytical signal

Sensitivities and peak characteristics. In general terms, when dealing with transient signals and, more specifically, in situations in which very low sample volumes are analyzed, the system must provide peaks as narrow as possible. Fig. 5 shows the peaks obtained for a nitric acid solution. The four sample introduction systems used in the present work were considered. It can be observed that, as was previously reported,[17] the TISIS (20 cm^3) gave rise to higher peaks than the double pass and Cinnabar spray chambers. The TISIS equipped with the 8 cm^3 cavity provided similar emission intensities as the two reference introduction systems. The most important advantage incorporated by TISIS (8 cm^3) was that it provided the narrowest peaks. The peak decay time was defined as the time elapsed until the signal dropped down to 1% of its maximum value. This parameter took values of 30, 12, 9 and 4 s for the double pass, Cinnabar, TISIS (20 cm^3) and TISIS (8 cm^3), respectively. These short decay times, measured at such low delivery rates, were obtained because no solution was aspirated between samples. As a consequence, processes such as sample plug dispersion in the conduction were minimized. The tailing of the peaks for the double pass spray chamber were mainly caused by the dispersion of the aerosol through its path towards the plasma.

The memory effects between samples were also studied. In the discrete sample introduction method used in the present work, memory effects were caused by re-nebulization of the analyte retained on the inner walls of the spray chamber coming from previous injections. In this case, several injections of the aqueous standard were performed. Afterwards, a 2 mol l^{-1} nitric acid solution having the same concentration of analyte was injected. For the double pass spray chamber three 10 μl sample injections were required to obtain the signals corresponding to the nitric acid solution. Beauchemin[7] found that two–three 100 μl injections of a 10 μg l^{-1} multielemental solution were required to completely wash the spray chamber after running the system with a 100 μg l^{-1} solution. For the Cinnabar, we observed that just one 10 μl injection was enough to wash the chamber. Meanwhile, for the TISIS (8 cm^3)

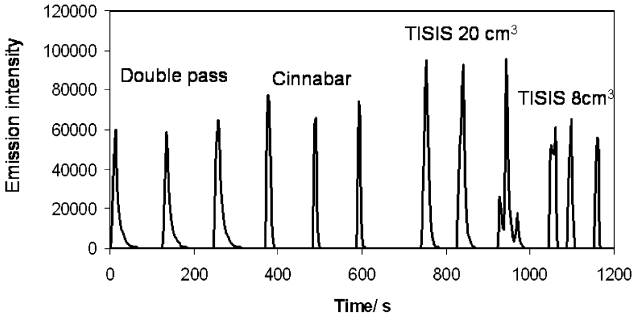

Fig. 5 ICP-AES peaks for the four systems tested in the present work obtained for a 2 mol l^{-1} nitric acid solution. Q_l = 30 μl min^{-1}; Q_g = 0.7 l min^{-1}; injected volume = 10 μl.

apparently there were no memory effects. The easy path towards the plasma imposed by the single pass spray chamber could be the reason for this trend.

Finally, Fig. 5 illustrates a problem that was found when the sample was injected into the air stream. The third signal for the TISIS with the 20 cm^3 cavity had, in fact, three peaks: the principal one surrounded by two additional shorter transient signals. By visual inspection it was found that the sample plug was dispersed into several small volumes during its path to the nebulizer. This problem was hardly found for the solutions used in the present work, although for some samples having low surface tension values (*e.g.*, ethanol–water mixtures) it was frequently observed.

Matrix effects. In the present work, the interferences caused by the matrices studied were evaluated by calculating the so-called relative intensity, I_{rel}, defined as:

$$I_{rel} = \frac{(I_{analyte})_{with\ matrix}}{(I_{analyte})_{without\ matrix}} \quad (6)$$

According to eqn. (6) a value of unity in I_{rel} meant that the matrix considered did not induce any change in analytical signal. Fig. 6 shows the I_{rel} values found for the double pass spray chamber (a), the Cinnabar (b) and the TISIS with the 8 cm^3 cavity (c). The matrix considered is 2 mol l^{-1} nitric acid. In general terms, the I_{rel} values were closer to unity in discrete than in continuous flow (*i.e.*, less pronounced interferences in the former case). When working in discontinuous mode, the spray chambers walls were kept dry. Therefore, once the primary aerosol was introduced into the spray chamber, the solvent evaporated primarily from the aerosol droplets, whereas in continuous mode it also evaporated from the inner chamber walls. This fact promoted the analyte transport to the plasma. As a result, the mass of analyte delivered to the excitation cell for plain water solutions and for nitric acid became similar and the interferences were therefore mitigated.

The results obtained with a sodium matrix (Fig. 7) agreed with those shown for nitric acid. The work in discrete sample introduction mode was more interesting for reducing the interferences in the case of the double pass spray chamber than for the other two systems. In this case, the interferences were virtually suppressed (*i.e.*, $I_{rel} \approx 1$) when sample injection in the air stream was applied. Interestingly, for the Cinnabar, the I_{rel} values were similar irrespective of the sample introduction mode used.

The improvement in I_{rel} when switching from continuous to discrete flow mode was more pronounced for the double pass spray chamber than for the other two systems tested. The data presented in Fig. 7 can be explained by taking into account two factors: *(i)*, in continuous mode the Cinnabar and TISIS were less sensitive to the matrix composition than the double pass spray chamber;[15,17] and *(ii)*, the aerosol residence time was longer for the double pass than for the remaining systems. At 0.7 l min^{-1}, the estimated gas residence times were about 0.7, 2 and 10 s for the TISIS (8 cm^3), Cinnabar and double pass,

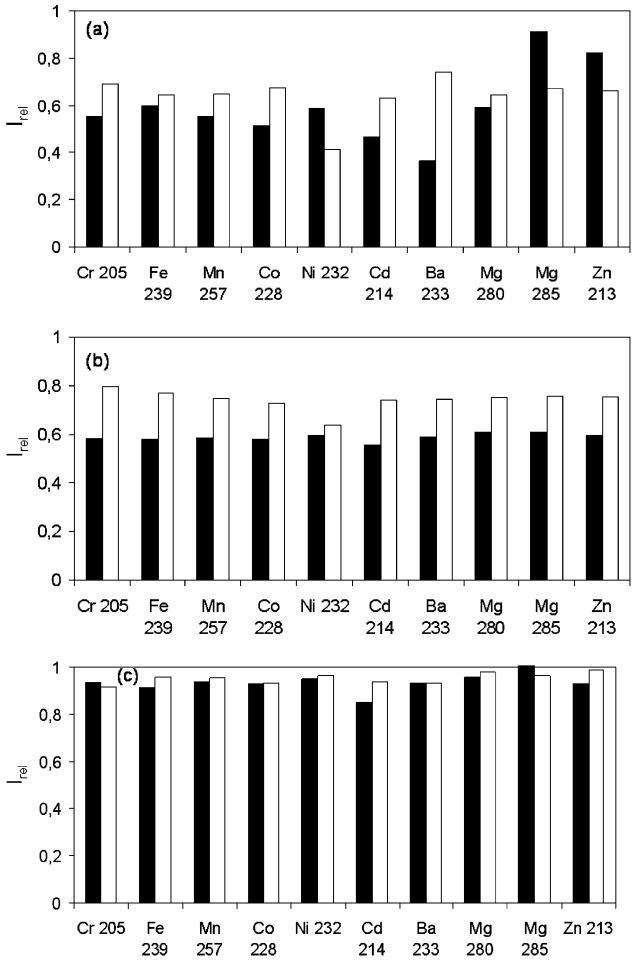

Fig. 6 Relative intensity, I_{rel}, for several emission lines obtained for a 2 mol l^{-1} nitric acid solution: (a) double pass spray chamber, (b) Cinnabar and (c) TISIS with the 8 cm^3 cavity. Black bars: continuous mode; white bars: sample injection in an air stream mode. Q_l = 20 µl min^{-1} (continuous) and 30 µl min^{-1} (discrete); injected volume = 10 µl; Q_g = 0.7 l min^{-1}.

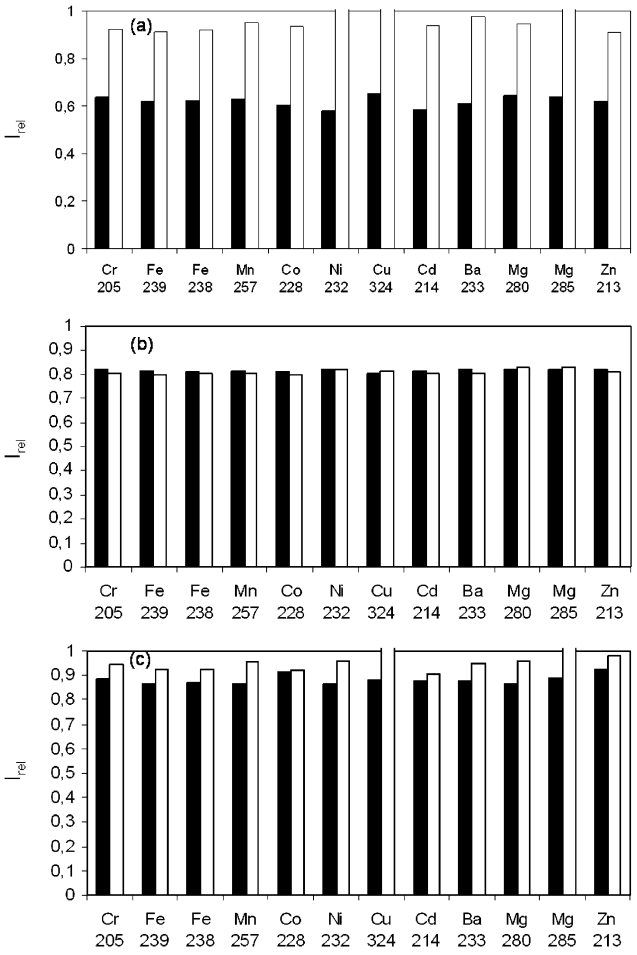

Fig. 7 Relative intensity, I_{rel}, for several emission lines obtained for a 5000 µg ml^{-1} sodium solution: (a) double pass spray chamber; (b) Cinnabar; and (c) TISIS with the 8 cm^3 cavity. Black bars: continuous mode; white bars: sample injection in an air stream mode. Q_l = 20 µl min^{-1} (continuous) and 30 µl min^{-1} (discrete); *I*njected volume = 10 µl; Q_g = 0.7 l min^{-1}.

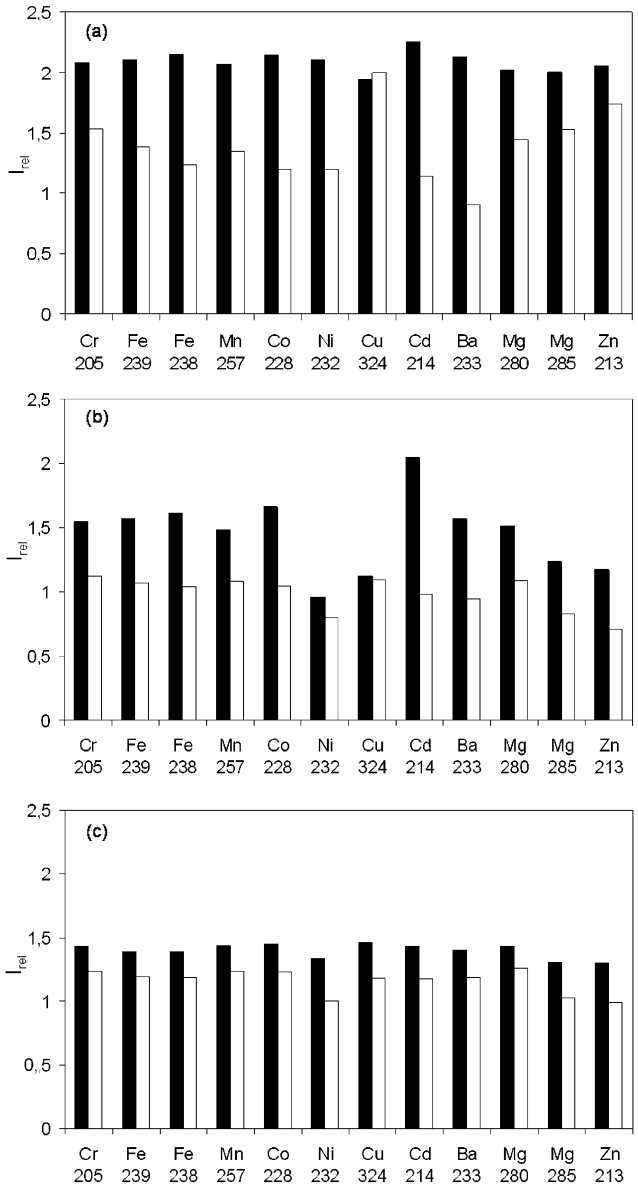

Fig. 8 Relative intensity, I_{rel}, for several emission lines obtained for a 1.7 mol l^{-1} acetic acid solution: (a) double pass spray chamber, (b) Cinnabar and (c) TISIS with the 8 cm^3 cavity. Black bars: continuous mode; white bars: sample injection in an air stream mode. Q_l = 20 µl min^{-1} (continuous) and 30 µl min^{-1} (discrete); *I*njected volume = 10 µl; Q_g = 0.7 l min^{-1}.

respectively. As a result, and in concordance with Figs. 3 and 4, the solvent evaporation was more significant for the double pass spray chamber both for water and matrices.

Unlike the situation with inorganic matrices, when working with organic acids such as acetic acid, the signal was higher than for a plain water standard;[19,25] thus I_{rel} was higher than 1 (Fig. 8). Again, the work in air injection mode appeared to mitigate the interferences. In other words, I_{rel} was closer to unity in discontinuous than in continuous flow. The intensification in the solvent evaporation from the aerosol in discrete sample introduction could also be argued to try to explain this behavior. When introducing plain water solutions, the evaporation was so intense that the mass of analyte transported to the excitation cell was close to that obtained in presence of acetic acid.

The plasma's thermal characteristics were evaluated by measuring the Mg II 280 nm to Mg I 285 nm line intensity ratio.[26] It has been claimed that a change in the energy transfer to the sample could be the origin of the sensitivity enhancement in air injection mode.[7] It was observed that, for inorganic matrices, the values of this relative parameter were of the same order (*i.e.*, close to 6) irrespective of the matrix and sample introduction considered. When considering a single peak, the Mg ratio in the zone of maximum peak intensity changed with time by roughly 10%, depending on the system and matrix. Therefore, the plasma's thermal characteristics were only slightly modified as the sample plug reached it. We could conclude that, for inorganic matrices, the interferences were virtually caused during the aerosol transport towards the excitation cell rather than in the plasma itself. However, for acetic acid, higher values of the Mg II to Mg I ratio were found (*i.e.*, ranging from 7 to 8). This trend has been already encountered in continuous mode[27] and indicated that, in the presence of acetic acid, the plasma thermal properties were significantly modified with respect to a plain water solution.

For most of the situations considered, the work in discrete mode showed itself to be useful in reducing the severity of the matrix effects caused by inorganic as well as organic compounds. However, a matrix effect was still present. Internal standardization was used to compensate for any residual effect. An important issue of internal standardization is the appropriate selection of the emission line acting as internal standard (IS). Several reports have highlighted the importance of the line characteristics on the efficiency of this technique.[28] Principal component analysis has allowed classification of the lines according to their efficiency as IS for eliminating interferences caused by easily ionized elements[29] and inorganic acids.[30,31] As indicated previously, the values of the Mg II to Mg I ratio did not change with the matrix considered and, as has been observed from Figs. 7 and 8, the plots of I_{rel} *versus* the line were quite flat; these findings suggested that the plasma was working under rather robust conditions.[32] In order to efficiently use the IS technique, a robust plasma should be used.[33] Furthermore, under these conditions, a single element could be used as IS for correcting for matrix effects on lines with very different energies. Hence, the peaks for the different elements were divided point by point by those corresponding to an element (acting as IS).[34] This procedure was followed for the plain water solution and for the nitric acid, sodium and acetic acid solutions.

Fig. 9 shows the ratio between the emission intensity for four different lines divided by that found for Mg (280.270 nm). The results are shown for the double pass spray chamber and the TISIS (8 cm^3) operated with the different matrices tested in the present work. As can be observed, in general terms, fairly flat responses were obtained throughout the peak. Several emission lines were used as internal standards, giving rise to similar results. Furthermore, the precision of the signal ratios was improved with respect to that for the peaks. Thus, for example, for the double pass spray chamber, the Mn (257.610 nm) peak height RSD (n = 5) was 4.4%, whereas the corresponding value of this parameter for the Mn to Cu 324.754 nm ratio was just 0.63%. In the absence of interferences, the value of the signal ratio should be equal irrespective of the matrix considered. The following equation was therefore applied to assess the efficiency of the internal standardization:

$$IS_{efficiency} = \frac{\left(\frac{I_{analyte}}{I_{IS}}\right)_{MATRIX}}{\left(\frac{I_{analyte}}{I_{IS}}\right)_{STANDARD}} \times 100 \qquad (7)$$

Table 4 shows the values of this parameter and compares them against the I_{rel} values (in percentage terms). It was found that, for inorganic matrices, when using Mg II 280 nm as IS, the $IS_{efficiency}$ value was closer to 100% than I_{rel}, which indicated that this was a good approach to remove matrix effects in discrete mode. As can be observed from Fig. 9, the values of $I_a/I_{Mg(280.270)}$ were nearly the same for almost all the elements, sample introduction systems and inorganic matrices.

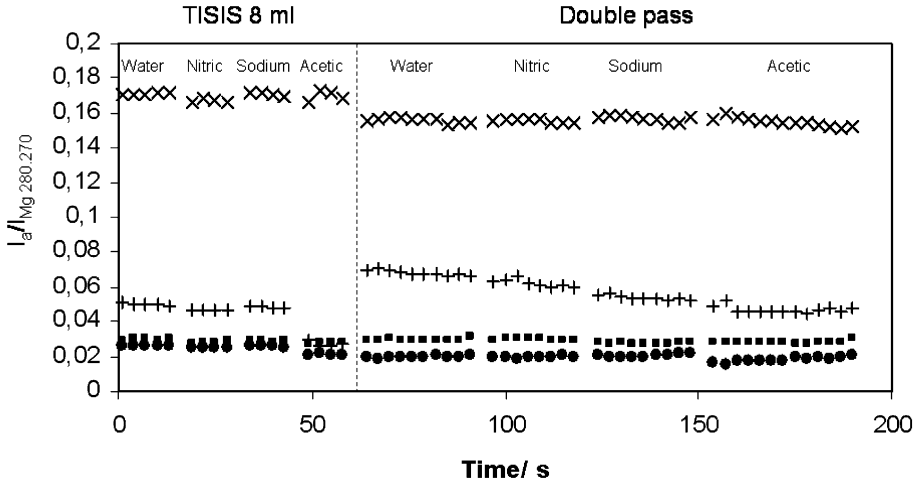

Fig. 9 Emission intensity (I_a) divided by that found for Mg 280.270 nm for two sample introduction systems, water and the three matrices tested. $Q_l = 30$ µl min^{-1}; $Q_g = 0.7$ l min^{-1}; injected volume = 10 µl. (●) Ba 233.527 nm; (■) Fe 239.562 nm; (×) Mn 257.610 nm; (+) Zn 213.856 nm.

In the present work, one atomic (*i.e.*, Cu 324.754 nm) and two ionic lines (*i.e.*, Co 228.616 nm and Cr 205.552 nm) were also used as IS. These lines behave better as IS for the Ni 232.003 line than Mg II. Thus, for the double pass spray chamber and Ni, the efficiency, taking nitric acid as the matrix, was virtually 100% (instead of 110%, Table 4) when using either the Co or the Cr line as IS. The results obtained were expected according to the work recently performed by Grotti and Frache.[30] In the case of the Mg I line, Cr and Cu provided efficiencies of about 99% instead of 108% (Table 4). For the rest of lines, the variation of efficiency *versus* the line taken as internal standard was less than 2%. In contrast, for the 5000 µg ml^{-1} sodium matrix, the Cu line provided the worst results with efficiencies that in most of the cases were close to 90%. The efficiency for Zn, in the case of the sodium matrix, was closest to 100% when the Cr line was used as IS.

Contrary to inorganic matrices, in the case of acetic acid, Mg II was not a good IS for five of the ten lines tested. Accordingly, Fig. 9 shows that, for acetic acid, Ba and Zn exhibited lower $I_a/I_{Mg(280.270)}$ values than those found for water, nitric acid and sodium. The results obtained were not significantly improved when using Cr, Cu or Co lines. Therefore, the origin of the acetic acid interference was, at least partially, in the analyte excitation step. As mentioned above, the Mg II to Mg I ratio was higher for acetic acid than for water.

Table 4 Comparison of I_{rel} with the efficiency of IS procedure[a]

	Double pass		TISIS (8 cm^3 cavity)	
	$IS_{efficiency}$ (%)	I_{rel} (%)	$IS_{efficiency}$ (%)	I_{rel} (%)
Matrix: nitric acid 2 mol l^{-1}				
Cr 205.552	98.6	67.4	98.5	94.4
Fe 239.562	96.5	59.9	96.0	92.8
Fe 238.204	98.2	53.6	95.5	92.7
Mn 257.610	99.9	55.6	98.1	95.4
Co 228.616	101.7	51.5	95.5	92.3
Ni 232.003	110.4	58.9	95.4	95.9
Cd 214.438	99.1	46.9	87.9	90.5
Ba 233.527	103.0	36.4	97.0	95.0
Mg 280.270	100	59.3	100	95.8
Mg 285.213	108.7	91.3	104.5	102.4
Zn 213.856	94.7	82.2	94.3	97.8
Average	101	60.3	96.6	95
Matrix: sodium 5000 µg ml^{-1}				
Cr 205.552	100.4	92.6	99.4	95.4
Fe 239.562	100.8	91.4	97.7	95.6
Fe 238.204	100.9	92.1	97.6	96.2
Mn 257.610	98.7	94.9	99.9	95.4
Co 228.616	101.0	93.5	98.6	96.9
Ni 232.003	100.4	114.8	100.7	96.0
Cd 214.438	97.4	94.0	95.7	97.0
Ba 233.527	98.0	97.9	98.9	95.0
Mg 280.270	100	94.8	100	95.8
Mg 285.213	99.6	109.7	103.6	102.4
Zn 213.856	90.9	91.0	98.3	97.8
Average	98.9	96.7	99.1	97.0
Matrix: acetic acid 1.7 mol l^{-1}				
Cr 205.552	102.1	154	100.9	124
Fe 239.562	96.9	139	94.6	120
Fe 238.204	98.3	124	94.7	119
Mn 257.610	97.6	135	99.7	123
Co 228.616	87.0	119	78.4	123
Ni 232.003	72.7	119	87.0	100
Cd 214.438	98.2	114	86.2	118
Ba 233.527	94.7	89.9	82.3	119
Mg 280.270	100	145	100	126
Mg 285.213	85.0	152	60.3	100
Zn 213.856	79.2	173	60.6	99
Average	92.0	133	85.9	116

[a] Internal standard: Mg 280.270 nm.

Analysis of reference certified samples

The data corresponding to the recoveries found for two food reference samples are summarized in Figs. 10 and 11 for the different sample introduction systems tested. Samples were spiked by adding 20 µl of a 1000 µg ml^{-1} multielemental solution to 10 g of the digested sample solution. In concordance with the results shown previously, the double pass spray chamber exhibited the highest sensitivity to the sample introduction mode. As expected from the data for inorganic matrices, higher recoveries were found in discrete than in continuous mode. However, the reported recoveries were always lower than 100%. Therefore, the internal standard procedure was applied. Table 5 shows the values relating to the efficiency of the IS procedure. Because, it was not detectable at the concentration present in the samples, and it behaved properly, we selected Cd 214.438 nm as internal standard. The results are compared against those of the recoveries found without IS. In this case, eqn. 4 was modified and the term referred to matrix corresponded to the spiked sample digested solutions. It can be observed that for reference materials, the IS efficiency also approached 100%.

Conclusions

Solvent evaporation from the aerosol is a significant process that can be promoted in order to try to mitigate non-spectroscopic interferences caused by inorganic as well as organic matrices in ICP-AES. A way of enhancing the evaporation is to introduce very low liquid sample volumes (*i.e.*, several

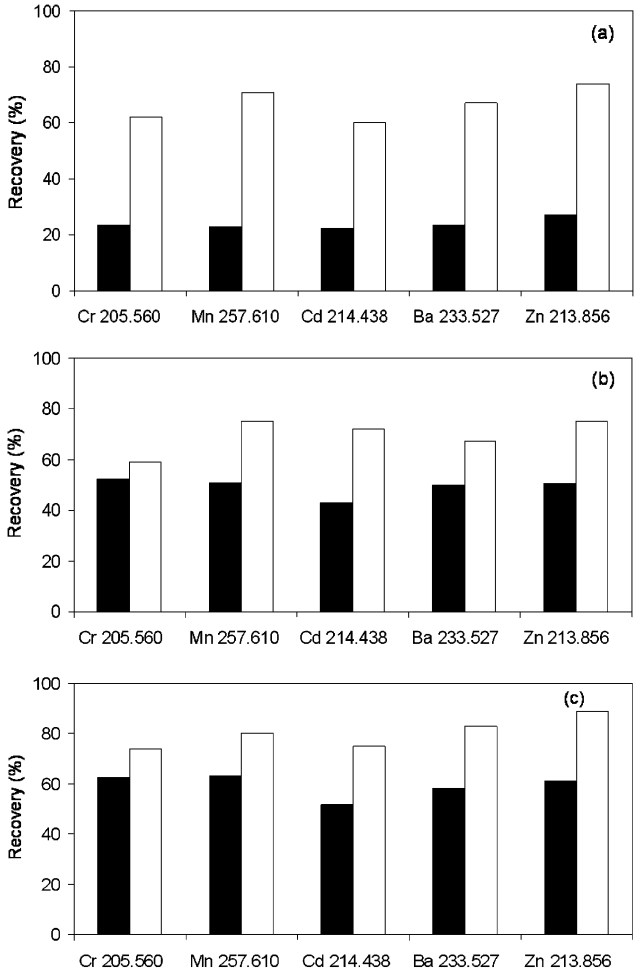

Fig. 10 Recoveries found for a bovine liver reference sample. (a) Double pass spray chamber, (b) Cinnabar and (c) TISIS equipped with the 8 cm^3 inner volume cavity. Black bars: continuous mode; white bars: sample injection in an air stream mode. Q_l = 30 µl min^{-1}; Q_g = 0.7 l min^{-1}; injected volume = 10 µl.

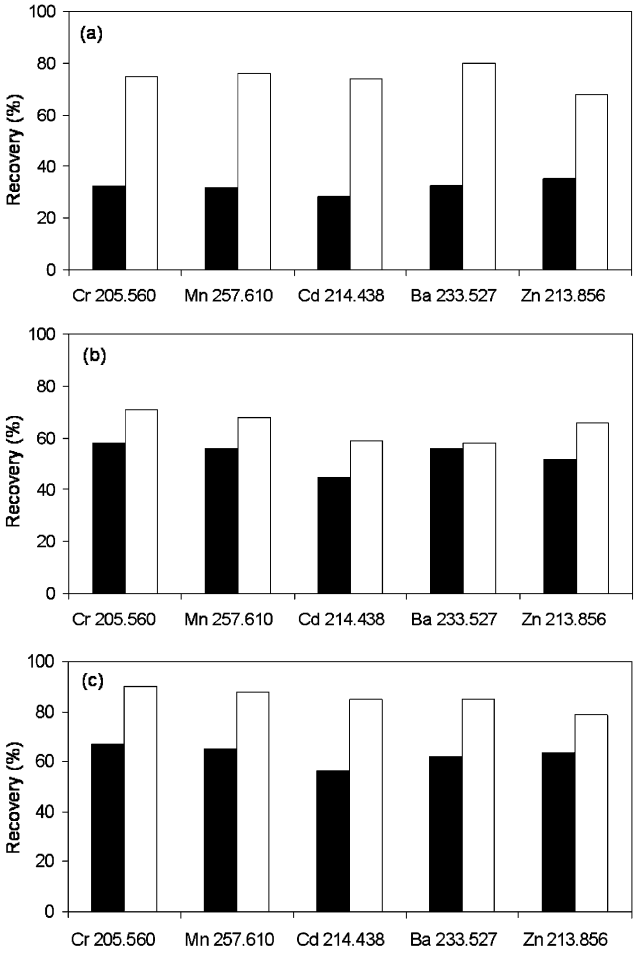

Fig. 11 Recoveries found for a mussel tissue reference sample. (a) Double pass spray chamber, (b) Cinnabar and (c) TISIS equipped with the 8 cm^3 inner volume cavity. Black bars: continuous mode; white bars: sample injection in an air stream mode. Q_l = 30 µl min^{-1}; Q_g = 0.7 l min^{-1}; injected volume = 10 µl.

microlitres) into a dry spray chamber. As a result of the evaporation of the solvent, the effect of the matrix on the mass of analyte entering the plasma per unit of time is less significant. The modification in the emission signal is therefore less significant than in continuous mode. In this second case, the solvent evaporates from the aerosol as well as from the spray chamber walls.

The predicted drop size characteristics from theoretical simulation, taking into account only solvent evaporation, differ from those obtained experimentally. The development of enhanced models for predicting the evaporation taking into

Table 5 Efficiency of the IS procedure and recoveries in discrete mode for the two solid reference materials tested[a]

	Double pass		Cinnabar		TISIS 1	
Emission line	$IS_{efficiency}$[b] (%)	Recovery[c] (%)	$IS_{efficiency}$[b](%)	Recovery[c](%)	$IS_{efficiency}$[b] (%)	Recovery[c] (%)
Bovine liver						
Li 670.781	90	62	99	82	102	91
Ba 233.527	92	67	89	67	83	66
Cr 205.552	109	73	98	59	85	74
Mn 257.610	102	71	104	75	105	80
Ni 231.604	97	50	95	66	98	72
Cu 324.754	93	50	88	48	100	65
Zn 213.856	113	74	95	75	112	89
Average	99.4	63.9	95.4	67.4	97.9	76.7
Mussel tissue						
Li 670.781	95	72	105	76	104	97
Ba 233.527	104	80	98	58	105	85
Cr 205.552	106	75	117	71	99	90
Mn 257.610	89	76	109	68	104	88
Ni 231.604	102	67	100	61	94	67
Cu 324.754	100	84	101	78	109	88
Zn 213.856	98	68	108	66	108	79
Average	99.1	74.6	105	68.3	103	82.0

[a] IS: Cd 214.438 nm. [b] Discrete mode. [c] Discrete mode without IS.

account issues such as the variation of the evaporation factor with time or modification in the drop size distribution by droplet coagulation are required to better understand the contribution of these processes to the overall matrix effect. Our findings also suggest that aerosol transport phenomena other than solvent evaporation are responsible for matrix effects.

The combination of discrete sample introduction into a dry environment and internal standardization is a powerful method for avoiding non-spectroscopic interferences in ICP-AES. In the present work, in order to carry out the calibration under the most difficult conditions, plain water standards were selected. Because the plasma was maintained under robust conditions, the selection of a suitable line to be used as internal standard was not critical, since a large number of them behave similarly in terms of the extent of the interference. Thus, a given line could efficiently compensate for signal variations caused by the matrix for lines with very different energies. The reliability of this method has been tested with reference solid samples by using a single internal standard.

Further studies on sample re-entrainment could be performed by studying: *(i)*, the effect of the duration between two pulses; and *(ii)*, the effect of the wettability by changing the cavity material (*e.g.*, Teflon or Ryton *versus* glass), or by adding non-ionic surfactant to improve the formation of a film.

The authors would like to thank to Mr. Eastgate (Glass Expansion, Europe) for the loan of the Cinnabar spray chamber and to Mr. Govaert (CPI International, The Netherlands) for the loan of the PFA pneumatic concentric nebulizer.

References

1 J. L. Todolí and J. M. Mermet, *Trends Anal. Chem.*, submitted for publication.
2 A. Montaser, M. G. Minnich, J. A. McLean, H. Liu, J. A. Caruso and C. W. McLeod, in *Inductively Coupled Plasma Mass Spectrometry*, ed. A. Montaser, Wiley-VCH, New York, 1998.
3 J. L. Todolí, S. Maestre, J. Mora, A. Canals and V. Hernandis, *Fresenius' J. Anal. Chem.*, 2000, **368**, 773.
4 M. Haldimann, A. Eastgate and B. Zimmerli, *Analyst*, 2000, **125**, 1977.
5 J. L. Todolí and J. M. Mermet, *J. Anal. At. Spectrom.*, 2002, **17**, 211.
6 A. Prange and D. Schaumlöffel, *J. Anal. At. Spectrom.*, 1999, **14**, 1329.
7 D. Beauchemin, *Analyst*, 1993, **118**, 815.
8 D. Beauchemin, D. C. Grégoire, D. Günther, V. Karanassios, J.-M. Mermet and T. J. Wood, *Discrete Sample Introduction Techniques for Inductively Coupled Plasma Mass Spectrometry*, Elsevier, Amsterdam, 2000.
9 B. F. Reis, M. A. Z. Arruda, E. A. G. Zagatto and J. R. Ferreira, *Anal. Chim. Acta*, 1988, **206**, 253.
10 J. M. Craig and D. Beauchemin, *Analyst*, 1994, **119**, 1677.
11 L. C. Tian, X. P. Sun, Y. Y. Xu and Z. L. Li, *Anal. Chim. Acta*, 1990, **238**, 183.
12 J. M. Craig and D. Beauchemin, *J. Anal. At. Spectrom.*, 1994, **9**, 1341.
13 V. Stefanova, V. Kmetov and L. Futekov, *J. Anal. At. Spectrom.*, 1997, **12**, 1271.
14 J. L. Todolí and J. M. Mermet, *J. Anal. At. Spectrom.*, 2002, **17**, 345.
15 J. L. Todolí and J. M. Mermet, *J. Anal. At. Spectrom.*, 2002, **17**, 913.
16 W. R. L. Cairns, C. Barbante, G. Capodaglio, P. Cescon, A. Gambado and A. Eastgate, *J. Anal. At. Spectrom.*, 2004, **19**, 286.
17 J. L. Todolí and J. M. Mermet, *J. Anal. At. Spectrom.*, 2003, **18**, 1185.
18 S. E. Maestre, J. L. Todolí and J. M. Mermet, *Anal. Bioanal. Chem.*, submitted for publication.
19 J. L. Todolí and J. M. Mermet, *Spectrochim. Acta, Part B*, 1999, **54**, 895.
20 I. I. Stewart and J. W. Olesik, *J. Anal. At. Spectrom.*, 1998, **13**, 843.
21 M. S. Cresser and R. F. Browner, *Spectrochim. Acta, Part B*, 1980, **35**, 73.
22 R. F. Browner, in *Inductively coupled plasma emission spectroscopy. Part II: Applications and fundamentals*, ed. P. W. J. M. Boumans, John Wiley and Sons, New York, 1987.
23 S. E. Maestre, J. Mora and J. L. Todolí, *Spectrochim. Acta, Part B*, 2002, **57**, 1753.
24 J. W. Olesik, J. A. Kinzer and B. Harkleroad, *Anal. Chem.*, 1994, **66**, 2002.
25 C. Dubuisson, E. Poussel, J. M. Mermet and J. L. Todolí, *J. Anal. At. Spectrom.*, 1998, **13**, 63.
26 J. M. Mermet, *Spectrochim. Acta, Part B*, 1989, **44**, 1109.
27 C. Dubuisson, E. Poussel, J. M. Mermet and J. L. Todolí, *J. Anal. At. Spectrom.*, 1998, **13**, 63.
28 A. Lopez-Molinero, A. Villareal-Caballero and J. R. Castillo, *Spectrochim. Acta, Part B*, 1994, **49**, 677.
29 M. Grotti, E. Magi and R. Leardi, *J. Anal, At. Spectrom.*, 2003, **18**, 274.
30 M. Grotti and R. Frache, *J. Anal. At. Spectrom.*, 2003, **18**, 1192.
31 I. B. Brenner, I. Segal, M. Mermet and J. M. Mermet, *Spectrochim. Acta, Part B*, 1995, **50**, 333.
32 C. Dubuisson, E. Poussel and J. M. Mermet, *J. Anal. At. Spectrom.*, 1997, **12**, 281.
33 C. Dubuisson, E. Poussel and J. M. Mermet, *J. Anal. At. Spectrom.*, 1998, **13**, 1265.
34 D. M. McCleathan, S. J. Ray and G. M. Hieftje, *J. Anal. At. Spectrom.*, 2001, **16**, 987.